27. Jeanpierre, M. Human satellites 2 and 3. *Ann. Genet.* **37,** 163–171 (1994).
28. Toyota, M. *et al.* Identification of differentially methylated sequences in colorectal cancer by methylated CpG island amplification. *Cancer Res.* **59,** 2307–2312 (1999).
29. Herman, J. G., Graff, J. R., Myohanen, S., Nelkin, B. D. & Baylin, S. B. Methylation-specific PCR: a novel PCR assay for methylation status of CpG islands. *Proc. Natl Acad. Sci. USA* **93,** 9821–9826 (1996).
30. Cameron, E. E., Bachman, K. E., Myohanen, S., Herman, J. G. & Baylin, S. B. Synergy of demethylation and histone deacetylase inhibition in the re- expression of genes silenced in cancer. *Nature Genet.* **21,** 103–107 (1999).

Supplementary information is available from *Nature*'s World-Wide Web site (http://www.nature.com) or as paper copy from the London editorial office of *Nature*.

Acknowledgements

We thank S. R. Lee and S. G. Rhee for sharing their expertise in HPLC analysis. We thank T. Chan, M. Esteller, N. Watkins and other members of our laboratories for helpful discussions. This work was supported by the Clayton Fund and by the National Institutes of Health. K.E.S. is a Fellow of the American Cancer Society.

Correspondence and requests for materials should be addressed to K.E.S. (e-mail: kornels@welchlink.welch.jhu.edu).

Direct observation of dendritic actin filament networks nucleated by Arp2/3 complex and WASP/Scar proteins

Laurent Blanchoin*, Kurt J. Amann*, Henry N. Higgs, Jean-Baptiste Marchand, Donald A. Kaiser & Thomas D. Pollard

Structural Biology Laboratory, Salk Institute for Biological Studies, 10010 N. Torrey Pines Road, La Jolla, California 92037, USA
** These authors contributed equally to this work*

Most nucleated cells crawl about by extending a pseudopod that is driven by the polymerization of actin filaments in the cytoplasm behind the leading edge of the plasma membrane[1,2]. These actin filaments are linked into a network by Y-branches, with the pointed end of each filament attached to the side of another filament and the rapidly growing barbed end facing forward[3]. Because Arp2/3 complex nucleates actin polymerization and links the pointed end to the side of another filament *in vitro*, a dendritic nucleation model has been proposed[4] in which Arp2/3 complex initiates filaments from the sides of older filaments. Here we report, by using a light microscopy assay, many new features of the mechanism. Branching occurs during, rather than after, nucleation by Arp2/3 complex activated by the Wiskott–Aldrich syndrome protein (WASP) or Scar protein; capping protein and profilin act synergistically with Arp2/3 complex to favour branched nucleation; phosphate release from aged actin filaments favours dissociation of Arp2/3 complex from the pointed ends of filaments; and branches created by Arp2/3 complex are relatively rigid. These properties result in the automatic assembly of the branched actin network after activation by proteins of the WASP/Scar family and favour the selective disassembly of proximal regions of the network.

We used fluorescence microscopy of filaments stained with fluorescent phalloidin (Figs 1 and 2) to establish the structural pathway of actin filament nucleation by Arp2/3 complex and to test the influence of profilin, capping protein, and nucleotide that is bound to actin monomers or actin filaments on the structure of the network. We focused on actin, Arp2/3 complex, capping protein and profilin, because they are ubiquitous[5], abundant, essential in genetic systems[6] and sufficient (with the addition of an actin-depolymerizing factor (ADF) or cofilin depolymerizing protein) to reconstitute *in vitro* assembly of actin filament comet tails that drive the motility of the intracellular bacteria, *Listeria* and *Shigella*[7]. Arp2/3 complex links the pointed ends of actin filaments to the sides of other filaments at an angle of 70° (ref. 4) and nucleates growth in the barbed direction when activated by the WA domains of WASP/Scar proteins[6]. Actin filaments potentiate nucleation by Arp2/3 complex that is activated by WASP/Scar proteins[8,9]. Arp2/3 complex is localized to 70° branches in the actin filament network at the leading edge of motile cells[10]. Capping protein and profilin have been proposed to maintain a pool of actin/profilin that is able to elongate free barbed ends but not pointed ends[11]. Profilin inhibits spontaneous actin nucleation more strongly than nucleation by Arp2/3 complex[8]. Capping protein also terminates the elongation of barbed ends[12] and efficiently nucleates actin filaments that grow in the pointed direction[13–15].

Light microscopy provides the first direct evidence that branching occurs during actin filament nucleation by Arp2/3 complex and WASP/Scar proteins (Fig. 1). Results are similar with highly purified Arp2/3 complex from *Acanthamoeba* and bovine thymus activated by WA domains from human WASP and Scar-1 (Table 1). On their own, actin monomers form nuclei spontaneously at a low rate (Fig. 1a), resulting in long and unbranched filaments (Fig. 1c, Table 1). Few branches form if WA-domain activated Arp2/3 complex is added after completion of spontaneous polymerization (Fig. 1d). Arp2/3 complex activated by WA domains accelerates the polymerization of Mg-ATP-actin (Fig. 1a), creates new filaments (Fig. 1b) and produces branches (Fig. 1e and f) depending on the concentrations of both components (Table 1). Branch length is inversely proportional to branch density because the concentration of actin subunits is limiting. The concentration of new barbed ends plateaus at high concentrations of Arp2/3 complex (Fig. 1b)[9], and, because nucleation is slower than elongation, actin monomers are consumed before each Arp2/3 complex can form a new filament. At high concentrations of activated Arp2/3 complex, branching is so dense that individual filaments cannot be resolved (data not shown). This is reminiscent of the densely branched filaments that are observed by electron microscopy in lamellipodia of keratocytes[3]. The mean lengths of actin filaments visualized by light microscopy are close to the lengths calculated from kinetic data (Table 1).

We determined the polarity of the filaments in branched networks by polymerizing Mg-ATP-actin monomers in the presence of rhodamine-phalloidin and preformed filaments labelled with Alexa green-phalloidin (Fig. 1j). In the absence of Arp2/3 complex, red unbranched actin filaments grow much longer at the barbed ends than at the pointed ends of the green filament seeds (Fig. 1j, left). In the presence of Arp2/3 complex and WASP/Scar proteins, the branches face the barbed ends, creating a polarized network (Fig. 1j, centre and right), as has been observed in cells by electron microscopy[3]. Dendritic nucleation occurs from the sides of ADP-P_i and ADP filaments with similar efficiency (Fig. 1j, centre and right). ADP-actin filaments were polymerized from ADP-actin monomers with green-phalloidin. ADP-P_i-actin filaments were polymerized from ATP-actin in the presence of green-phalloidin, which inhibits phosphate release. These filaments were added to ATP-actin monomers, activated-Arp2/3 complex and red phalloidin to label the new filaments. With ADP$_i$-actin filaments, 70% of the branches grew from the initial filaments, 30% from the new ATP-actin filaments. With ADP-P_i-actin filaments, 50% of the branches grew from the initial filaments. In biochemical experiments, ADP-actin and ATP-actin filaments enhance nucleation by Arp2/3 complex to the same extent[9].

Nucleotide bound to actin has two marked effects on branching that are probably related mechanistically. First, ADP-actin monomers polymerize but rarely form branches in the presence of high concentrations of activated Arp2/3 complex (Fig. 1g). Second, the branching density of Mg-ATP-actin that is polymerized in the

presence of activated Arp2/3 complex depends on when rhodamine-phalloidin is added to the sample. Branching is maximal if rhodamine-phalloidin is present during polymerization. If added 20 min later, fewer branches are observed (Fig. 1h) unless BeF_3 is included (Fig. 1i). Because phalloidin inhibits phosphate release from ADP-P_i-actin filaments[16] and BeF_3 stabilizes a state similar to ADP-P_i (ref. 17), ATP-actin and ADP-P_i-actin subunits probably favour the formation and maintenance of branches. ATP hydrolysis and phosphate dissociation may thus provide an automatic timer to initiate the disassembly of the branched network (Fig. 3).

The combination of Arp2/3 complex, capping protein and profilin strongly favours branched nucleation (Fig. 2b and d; and Table 1), creating many more short branches than in the absence of capping protein (Fig. 2a and c). Polymerization of actin with capping protein produces many short filaments that are capped on their barbed ends[13,15]. Inclusion of profilin with activated Arp2/3 complex and capping protein suppresses both nucleation by capping protein and pointed-end growth from capped filaments, but allows branching nucleation by Arp2/3 complex. Capping protein rapidly terminates these new filaments. This preserves the subunit pool and produces densely branched networks (Fig. 2b and d). This is a striking example of the cooperation of the multiple components in this complicated system.

High-speed imaging of branched actin filaments undergoing thermal fluctuations (Fig. 2e–n) revealed that the Y-junctions created by Arp2/3 complex are stiff. The mean (± s.d.) angle measured 0.5–1 μm from the Y-junction in 400 frames of several branches was 77° (± 13°) for bovine Arp2/3 complex and 71° (± 10°) for amoeba Arp2/3 complex, which corresponds to rotational spring constants of 7.6×10^{-20} J rad^{-2} and 13×10^{-20} J rad^{-2}, respectively. The narrow angular distribution suggests that branches produced by Arp2/3 complex are sufficiently rigid to be compatible with the elastic Brownian ratchet model[18] for growing actin filaments pushing forward a membrane or a bacterium.

Light microscopy is an ideal approach to study the formation and dynamics of the branched actin network that is generated by

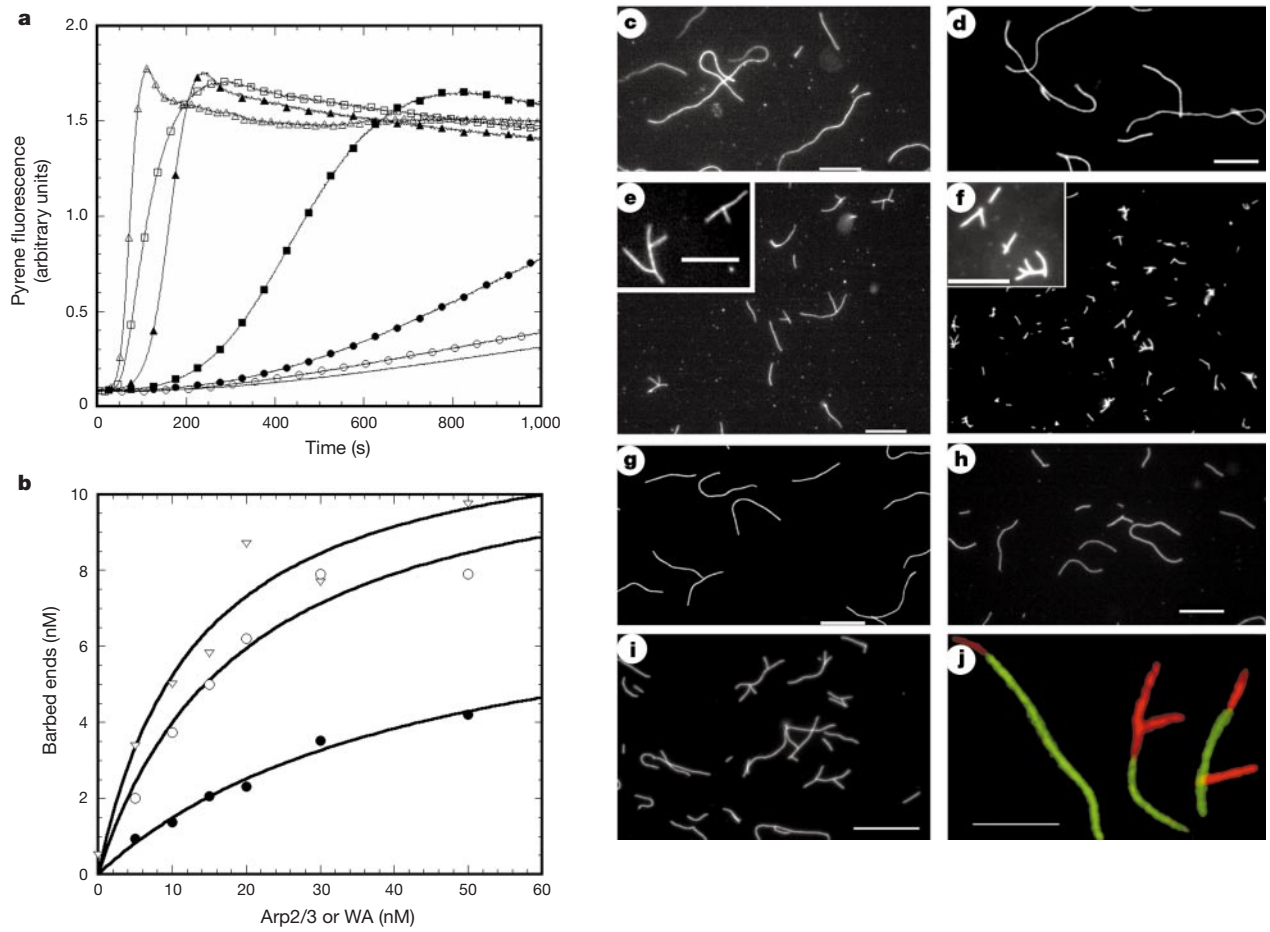

Figure 1 Comparison of the kinetics of actin polymerization in the presence of Arp2/3 complex and WASP WA domain with the structure of the products observed by light microscopy. **a**,**b**, Biochemical assays. Conditions: 4 μM actin (5% pyrene-labelled), 10 mM imidazole pH 7, 50 mM KCl, 1 mM $MgCl_2$, 1 mM EGTA, 0.5 mM dithiothreitol, 0.1 mM $CaCl_2$, 0.2 mM ATP and 3 mM NaN_3, 22 °C. **a**, Time course of polymerization monitored by pyrene fluorescence. Line with no symbols, no additions to actin. Filled symbols, experiments with 100 nM amoeba Arp2/3 complex and varying concentrations of human Scar WA: filled circles, no WA; filled squares, 5 nM WA; filled triangles, 50 nM WA. Open symbols, experiments with 100 nM human Scar WA and varying concentrations of Arp2/3 complex: open circles, no Arp2/3 complex; open squares, 5 nM Arp2/3 complex; open triangles, 50 nM Arp2/3 complex. **b**, Concentrations of barbed ends[9]. Open triangles, 100 nM WASP-WA with variable bovine Arp2/3 complex; open circles, 100 nM Scar-WA with variable amoeba Arp2/3 complex; filled circles, 100 nM amoeba Arp2/3 complex with variable Scar-WA. **c**–**i**, Fluorescence micrographs of the products of actin polymerization as a function of Arp2/3 complex and WASP. **c**, Mg-ATP-actin alone; **d**, 20 nM of bovine Arp2/3 complex and 100 nM of WASP-WA added to the actin filament mixture after polymerization; **e**, Mg-ATP-actin polymerized with 15 nM bovine Arp2/3 complex and 100 nM WASP-WA; **f**, Mg-ATP-actin polymerized with 50 nM bovine Arp2/3 complex and 100 nM WASP-WA; **g**, Mg-ADP-actin polymerized with 50 nM bovine Arp2/3 complex and 400 nM WASP-WA; **h**, as **e** but phalloidin added after 20 min; **i**, as **h** but in the presence of 150 μM $BeCl_2$ and 5 mM NaF; **j**, as **e** but in presence of 300 nM polymerized actin previously labelled with Alexa green phalloidin. Scale bars, 10 μm for **c**–**i** and 2.5 μm for **j**.

dendritic nucleation in the presence of Arp2/3 complex. This approach cannot assess the components that are required for bacterial motility as can a reconstitution assay[7], but the visualization of individual filaments provides more insights into the molecular mechanisms, which we summarize in a revised dendritic nucleation model (Fig. 3).

In our experiments and in cells, new filaments arise from a pool of Mg-ATP-actin monomers that are bound to profilin, which suppresses spontaneous nucleation. Existing filaments are mostly capped on their barbed ends by capping protein and on their pointed ends by Arp2/3 complex. Activation of Arp2/3 complex by a WASP/Scar protein initiates the assembly of a new filament (step 1). Branching is tightly coupled to nucleation (step 2). Arp2/3 complex may bind the side of a pre-existing filament before nucleation of a new filament, because preformed filaments stimulate nucleation[8] and a lag occurs at the onset of polymerization of pure actin monomers, even with high concentrations of activated Arp2/3 complex[9]. The pool of Mg-ATP-actin/profilin rapidly elongates the new barbed end (step 3), and the stiff, elastic filament anchored at its pointed end by a rigid branch pushes forward the plasma membrane (step 4). Elongation is transient, because growth is terminated by binding of capping protein (step 5). Profilin and capping protein enhance branching and limit the length of the new filaments. Profilin suppresses spontaneous nucleation more effectively than branching nucleation by Arp2/3 complex[8], and capping protein terminates growth before the pool of subunits is depleted[12]. Unexpectedly, the nucleotide that is bound to actin monomers and filaments influences dendritic nucleation and the stability of branches. The simplest interpretation of our observations is that ATP hydrolysis and phosphate release (step 6) weaken the interaction of the pointed end of the new filament with Arp2/3 complex (step 7) (R. D. Mullins, personal communication). This may be the first step in the disassembly of the new filament. ADF/cofilins promote this step by catalysing phosphate release[19]. These proteins

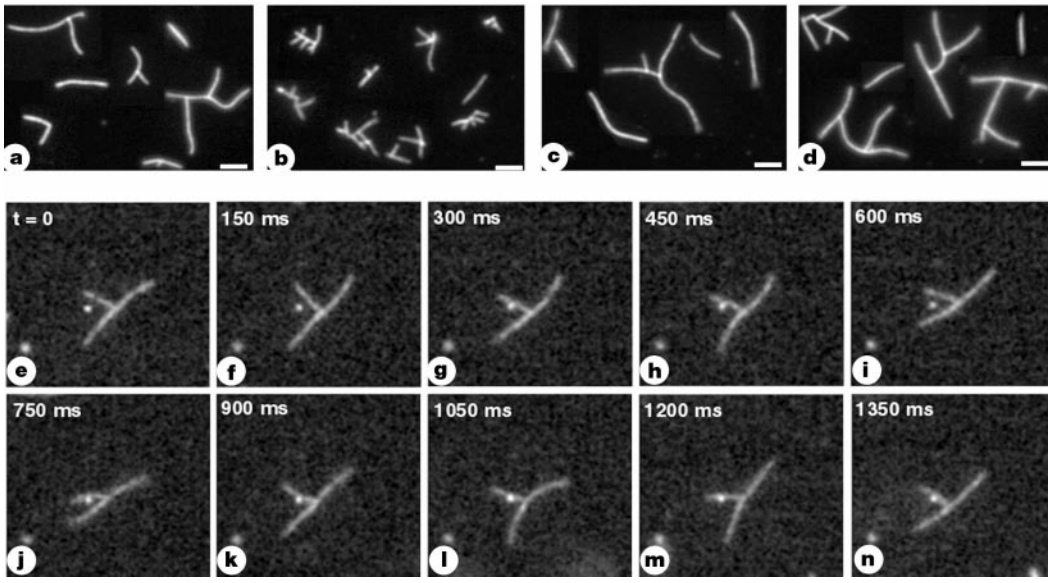

Figure 2 Regulation of branch length and observation of branch point rigidity. **a**–**d**, Effect of Arp2/3 complex and capping protein on actin polymerization. Polymerization conditions: 4 μM actin monomers, 15 nM Arp2/3 complex, 100 nM WA, 50 mM KCl, 1 mM $MgCl_2$, 1 mM EGTA, 0.5 mM DTT, 0.1 mM $CaCl_2$, 3 mM NaN_3, 10 mM imidazole pH 7.0 and 4 μM rhodamine-phalloidin. **a**,**b**, Amoeba actin and 16 μM amoeba profilin-I were polymerized alone (**a**), or with 100 nM amoeba capping protein (**b**). **c**,**d**, Muscle actin and 8 μM human profilin were polymerized alone (**c**), or with 60 nM amoeba capping protein (**d**). Scale bar, 2.5 μm. **e**–**n**, Thermal fluctuations of branched actin filaments formed from 4 μM muscle actin, 15 nM Arp2/3 complex, 100 nM WASP-WA and 4 μM rhodamine-phalloidin and diluted into fluorescence buffer as in Fig. 1. Fluorescence micrographs were recorded at 15-ms intervals. Every tenth frame illustrates the stiffness of the branch point relative to the flexibility of the filament. Branch length 2 μm.

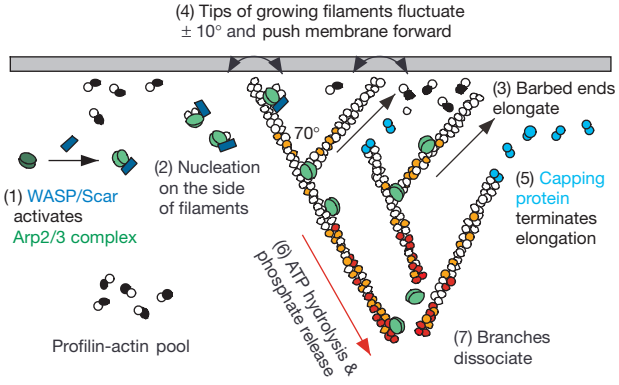

Figure 3 Model for the assembly and disassembly of the dendritic actin filament network at the leading edge of a cell. ATP-actin is shown in white, ADP-P-actin in orange, ADP-actin in red, and profilin in black.

Table 1 Quantitation of branching and filament length

Arp2/3 (nM)	WA (nM)	CP (nM)	Profilin (μM)	Biochemical length (μm)	Microscopic length (μm)	Branching (%)
Amoeba system: co-polymerization of Mg-ATP actin with rhodamine-phalloidin						
0	100	0	0		12.0 ± 10	0
5	100	0	0	6.5	7.8 ± 0.7	28
50	100	0	0	1.6	1.3 ± 0.5	97
15	100	0	16		2.4 ± 1.1	73
15	100	100	16		1.3 ± 0.6	91
Mammalian system: co-polymerization of Mg-ATP actin with rhodamine-phalloidin						
0	0	0	0	21	19.7 ± 13	0
10	100	0	0	2.6	6.6 ± 6	14
15	100	0	0		3.2 ± 2.2	56
50	100	0	0	1.4	2.3 ± 1.7	90
15	100	0	8		10.3 ± 10	8.3
15	100	60	8		5.8 ± 4.6	43
Addition of rhodamine-phalloidin after 20 min polymerization of Mg-ATP actin						
15	100	0	0		4.8 ± 4	12
Addition of rhodamine-phalloidin after 20 min polymerization of Mg-ATP actin with BeF_3						
15	100	0	0		3.8 ± 4.2	42
Co-polymerization Mg-ATP actin with rhodamine-phalloidin; addition of Arp2/3 complex after 20 min						
15	100	0	0		15.0 ± 9.8	3
Co-polymerization of Mg-ADP actin with rhodamine-phalloidin						
60	400	0	0		12.6 ± 9.0	8

Protein sources: Amoeba actin was tested as indicated with amoeba Arp2/3 complex, human Scar-WA and amoeba profilin-1; and rabbit skeletal muscle actin was tested as indicated with bovine Arp2/3 complex, human WASp-WA and human profilin-I. CP, amoeba capping protein. Biochemical lengths are calculated as described[9]. Microscopic lengths are given with standard deviations. At least 100 individual filaments from 2 to 5 different experiments were observed for all length and branching measurements. Conditions: 4 μM actin with the indicated nucleotide, 4 μM rhodamine-phalloidin, 50 mM KCl, 1 mM $MgCl_2$, 1 mM EGTA, 10 mM imidazole pH 7.0, 1 mM ATP or ADP as indicated, 22 °C, for 20 min before dilution into fluorescence buffer and preparation of slides.

also sever ADP-actin filaments[20] and dissociate ADP-actin subunits from filament ends[21]. Further investigation of each of these steps will bring us closer to understanding the mechanism of force generation by actin polymerization during cell motility. □

Methods

Protein purification

Actin was purified from rabbit skeletal muscle acetone powder[22] or from *Acanthamoeba*[23], Arp2/3 complex from bovine thymus[9] or from *Acanthamoeba*[24], capping protein from *Acanthamoeba*[24], profilin from *Acanthamoeba*[26]. Human profilin was bacterially expressed and purified[27]. Actin was labelled on Cys 374 to a stoichiometry of 0.9–1.0 with pyrene iodoacetamide[23,28]. Human WASP-WA domain was expressed and purified as described[8]. Human Scar-WA domain was bacterially expressed and purified by gel filtration (G50) followed by DEAE chromatography.

Polymerization

Actin was polymerized by addition of a 1:9 dilution of 10× KMEI (500 mM KCl, 10 mM $MgCl_2$, 10 mM EGTA, 100 mM imidazole, pH 7). Actin polymerization in presence of Arp2/3 complex and WASP-WA domain has been described[9].

Microscopy

After 20 min of polymerization at 22 °C in presence of rhodamine-phalloidin or Alexa green phalloidin, actin was diluted to a final concentration of 10 nM in fluorescence buffer containing 50 mM KCl, 1 mM $MgCl_2$, 100 mM dithiothreitol, 20 μg ml^{-1} catalase, 100 μg ml^{-1} glucose oxidase, 3 mg ml^{-1} glucose, 0.5% methylcellulose, 10 mM imidazole pH 7.0. Two microlitres were applied to coverslips coated in 0.1% nitrocellulose and fluorescence viewed with an Olympus IX-70 microscope using a mercury illumination source. Images were collected using a Hamamatsu digital camera. Filament lengths, branch number and angles were measured manually using Metamorph software. The rotational spring constant of branches was calculated from the equation, $\kappa(\theta)^2 = kT$, based on the equipartition principle, where κ is the rotational spring constant, θ is the standard deviation of the angle (in radians) and kT is the thermal energy (4×10^{-21} J).

Received 30 December 1999; accepted 15 February 2000.

1. Wang, Y. Exchange of actin subunits at the leading edge of living fibroblasts: possible role of treadmilling. *J. Cell Biol.* **101,** 597–602 (1985).
2. Theriot, J. A. & Mitchison, T. J. Actin microfilament dynamics in locomoting cells. *Nature* **352,** 126–131 (1991).
3. Svitkina, T. M., Verkhovsky, A. B., McQuade, K. M. & Borisy, G. G. Analysis of the actin-myosin II system in fish epidermal keratocytes: mechanism of cell body translocation. *J. Cell Biol.* **139,** 397–415 (1997).
4. Mullins, R. D., Heuser, J. A. & Pollard, T. D. The interaction of Arp2/3 complex with actin: nucleation, high-affinity pointed end capping, and formation of branching networks of filaments. *Proc. Natl Acad. Sci. USA* **95,** 6181–6186 (1998).
5. Pollard, T. D. in *Guidebook to the Cytoskeletal and Motor Proteins* 2nd edn (eds Kreis, T. & Vale, R.) 3–11 (1999).
6. Higgs, H. N. & Pollard, T. D. Regulation of actin polymerization by Arp2/3 complex and WASP/Scar proteins. *J. Biol. Chem.* **274,** 32531–32534 (1999).
7. Loisel, T. P., Boujemaa, R., Pantaloni, D. & Carlier, M. F. Reconstitution of actin-based motility of *Listeria* and *Shigella* using pure proteins. *Nature* **401,** 613–616 (1999).
8. Machesky, L. M. *et al.* Scar, A WASP-related protein, activates nucleation of actin filaments by the Arp2/3 complex. *Proc. Natl Acad. Sci. USA* **96,** 3739–3744 (1999).
9. Higgs, H. N., Blanchoin, L. & Pollard, T. D. Influence of the Wiskott–Aldrich syndrome protein (WASP) C terminus and Arp2/3 complex on actin polymerization. *Biochemistry* **38,** 15212–15222 (1999).
10. Svitkina, T. M. & Borisy, G. G. Arp2/3 complex and actin depolymerizing factor/cofilin in dendritic organization and treadmilling of actin filament array in lamellipodia. *J. Cell Biol.* **145,** 1009–1026 (1999).
11. Pollard, T. D. & Cooper, J. A. Quantitative analysis of the effect of *Acanthamoeba* profilin on actin filament nucleation and elongation. *Biochemistry* **23,** 6631–6641 (1984).
12. Schafer, D. A., Jennings, P. B. & Cooper, J. A. Dynamics of capping protein and actin assembly *in vitro*: uncapping barbed ends by polyphosphoinositides. *J. Cell Biol.* **135,** 169–179 (1996).
13. Cooper, J. A. & Pollard, T. D. Effects of capping protein on the kinetics of actin polymerization. *Biochemistry* **24,** 793–799 (1985).
14. Caldwell, J. E., Heiss, S. G., Mermall, V. & Cooper, J. A. Effects of CapZ, an actin capping protein of muscle, on the polymerization of actin. *Biochemistry* **28,** 8506–8514 (1989).
15. Xu, J., Casella, J. F. & Pollard, T. D. Effect of capping protein, CapZ, on the length of actin filaments and mechanical properties of actin filament networks. *Cell. Motil. Cytoskeleton* **42,** 73–81 (1999).
16. Dancker, P. & Hess, L. Phalloidin reduces the release of inorganic phosphate during actin polymerization. *Biochim. Biophys. Acta* **1035,** 197–200 (1990).
17. Combeau, C. & Carlier, M. F. Characterization of the aluminum and beryllium fluoride species bound to F-actin and microtubules at the site of the g-phosphate of the nucleotide. *J. Biol. Chem.* **264,** 19017–19021 (1989).
18. Mogilner, A. & Oster, G. Cell motility driven by actin polymerization. *Biophys. J.* **71,** 303–345 (1996).
19. Blanchoin, L. & Pollard, T. D. Mechanism of interaction of *Acanthamoeba* actophorin (ADF/cofilin) with actin filaments. *J. Biol. Chem.* **274,** 15538–15546 (1999).
20. Maciver, S. K., Zot, H. G. & Pollard, T. D. Characterization of actin filament severing by actophorin from *Acanthamoeba castellanii*. *J. Cell Biol.* **115,** 1611–1620 (1991).
21. Carlier, M. F. *et al.* Actin depolymerizing factor (ADF/cofilin) enhances the rate of filament turnover: implication in actin-based motility. *J. Cell Biol.* **136,** 1307–1322 (1997).
22. Spudich, J. A. & Watt, S. The regulation of rabbit skeletal muscle contraction. Biochemical studies of the interaction of the tropomyosin–troponin complex with actin and the proteolytic fragments of myosin. *J. Biol. Chem.* **246,** 4866–4871 (1971).
23. Pollard, T. D. Polymerization of ADP-actin. *J. Cell Biol.* **99,** 769–777 (1984).

24. Machesky, L. M., Atkinson, S. J., Ampe, C., Vandekerckhove, J. & Pollard, T. D. Purification of a cortical complex containing two unconventional actins from *Acanthamoeba* by affinity chromatography on profilin agarose. *J. Cell Biol.* **127,** 107–115 (1994).
25. Cooper, J. A., Blum, J. D. & Pollard, T. D. *Acanthamoeba castellanii* capping protein: properties, mechanism of action, immunologic cross-reactivity, and localization. *J. Cell Biol.* **99,** 217–225 (1984).
26. Kaiser, D. A., Goldschmidt-Clermont, P. J., Levine, B. A. & Pollard, T. D. Characterization of renatured profilin purified by urea elution from poly-L-proline agarose columns. *Cell Motil.* **14,** 251–262 (1989).
27. Almo, S. C., Pollard, T. D., Way, M. & Lattman, E. E. Purification, characterization and crystallization of *Acanthamoeba* profilin expressed in *Escherichia coli*. *J. Mol. Biol.* **236,** 950–952 (1994).
28. Kouyama, T. & Mihashi, K. Fluorimetry study of N-(1-pyrenyl) iodoacetamide-labelled F-actin. Local structural change of actin protomer both on polymerization and on binding of heavy meromyosin. *Eur. J. Biochem.* **114,** 33–38 (1981).

Acknowledgements

This work was supported by an NIH research grant to T.D.P., fellowships from National Research Service Award to K.J.A. and H.N.H. and from the Association pour la Recherche contre le Cancer to J.B.M. We thank J. Howard for advice on calculating the spring constant.

Correspondence and requests for materials should be addressed to T.D.P. (e-mail: pollard@salk.edu).

Low fidelity DNA synthesis by human DNA polymerase-η

Toshiro Matsuda*, Katarzyna Bebenek*, Chikahide Masutani†, Fumio Hanaoka†‡ & Thomas A. Kunkel*§

** Laboratory of Molecular Genetics and § Laboratory of Structural Biology, National Institute of Environmental Health Sciences, Research Triangle Park, North Carolina 27709, USA*
† Institute for Molecular and Cellular Biology, Osaka University and CREST, Japan Science and Technology Corporation, 1-3 Yamada-oka, Suita, Osaka 565-0871, Japan
‡ RIKEN, Wako-shi, Saitama 351-0198, Japan

A superfamily of DNA polymerases that bypass lesions in DNA has been described[1–4]. Some family members are described as error-prone because mutations that inactivate the polymerase reduce damage-induced mutagenesis. In contrast, mutations in the skin cancer susceptibility gene *XPV*[5,6], which encodes DNA polymerase (pol)-η, lead to increased ultraviolet-induced mutagenesis[7–11]. This, and the fact that pol-η primarily inserts adenines during efficient bypass of thymine–thymine dimers *in vitro*[8,12,13], has led to the description of pol-η as error-free. However, here we show that human pol-η copies undamaged DNA with much lower fidelity than any other template-dependent DNA polymerase studied. Pol-η lacks an intrinsic proofreading exonuclease activity and, depending on the mismatch, makes one base substitution error for every 18 to 380 nucleotides synthesized. This very low fidelity indicates a relaxed requirement for correct base pairing geometry and indicates that the function of pol-η may be tightly controlled to prevent potentially mutagenic DNA synthesis.

The ability of pol-η to bypass efficiently a DNA adduct that usually blocks synthesis by other polymerases indicates that pol-η may have relaxed discrimination ability. To test this hypothesis, we examined the fidelity of human pol-η during copying of undamaged DNA. Recombinant pol-η containing a carboxy-terminal hexahistidine tag[5] was first examined for the presence of exonuclease activities using a 5′-end labelled template primer containing a 3′-terminal A·dGMP mismatch[14]. Neither 5′ → 3′ nor 3′ → 5′ exonuclease activities were detected (Fig. 1a, lane 2). Thus, pol-η lacks an intrinsic exonuclease activity that can proofread replication errors. We then investigated the fidelity of pol-η during synthesis to fill a five-nucleotide gap with an undamaged DNA template containing a TGA nonsense codon in the *LacZ* gene in M13mp2 DNA[15]. This substrate encodes a colourless M13 plaque phenotype, and errors are scored as blue revertant plaques when the DNA products are introduced into an α-complementation strain of *Escherichia coli* and plated on indicator plates.

Synthesis by pol-η generated gap-filled products (not shown, but see ref. 15 and below) whose revertant frequency was 8,400-fold higher than that of control DNA that had not been copied *in vitro* (Table 1). DNA sequence analysis revealed that 8 of 12 revertants contained a single base substitution and that the other 4 contained 2 substitutions among the 5 nucleotides copied. Both the high reversion frequency and the number of revertants containing multiple substitutions indicate that pol-η has low fidelity. The base substitution error rate calculated from these data is $3{,}100 \times 10^{-5}$ (1 error in 32 bases, 1/32). This rate is 24-fold higher than for human DNA polymerase-β (Table 1), the least accurate among wild-type DNA polymerases that have previously been studied.

To determine whether such low fidelity is site-specific or a general feature of synthesis by pol-η, we used a 407-nucleotide gap that permits detection of hundreds of different substitution, addition, deletion and complex errors generated when copying a 275-nucleotide sequence of the wild-type *LacZ* α-complementation gene[16]. Here, errors are scored as light-blue or colourless mutant plaques and the error specificity is defined by sequence analysis of independent *lacZ* mutants. Analysis of the DNA products of gap-filling synthesis revealed that pol-η filled the 407-nucleotide gap (Fig. 1b, lane 2). These products yielded a *lacZ* mutant frequency of 32%, a value that is unprecedented in comparison with the 0.1 to 3% values obtained with other wild-type, template-dependent DNA polymerases (Table 1). Similar values were observed for synthesis using 10- and 100-fold lower dNTP concentrations or for reactions containing 2- or 4-fold less pol-η. The average mutant frequency for six independent determinations was 34% (Table 1).

In contrast to the predominantly light-blue phenotypes of *lacZ* mutants generated by most other DNA polymerases using this assay, more than 95% of the pol-η-dependent *lacZ* mutants had a colourless rather than light-blue plaque phenotype. Sequence analysis of 24 *lacZ* mutants revealed that they contained from 3 to 22 changes per mutant. A total of 232 single base substitutions, 10 tandem double-base substitutions, 13 additions of 1–3 nucleotides and 32 deletions of 1–56 nucleotides were observed. The recovery of 232 single base substitutions among only 6,600 total nucleotides analysed (24 mutants × 275 nucleotides) yields an average base

Table 1 Fidelity of human pol-η

DNA polymerase	Polymerase family	3′-exo activity	Mutant frequency* (×10^{-4})	Average base substitution rate (×10^{-5})†
TGA codon reversion assay			0.05 (control‡)	
Pol-η	Rad30	no	420	3,100
Pol-β	Pol X	no	26	130§
Forward mutation assay			6 (control‡)	
Pol-η	Rad30	no	3,400	3,500
Pol-β	Pol X	no		67
Pol-α	Pol α	no		16
HIV-1 RT	RT	no		6
E. coli Kf pol	Pol I	no‖		2
Pol-δ	Pol α	yes		~1
Pol-ε	Pol α	yes		≤1
Pol-γ	Pol I	yes		≤1

* The reversion frequency is the average of two determinations; the forward mutant frequency is the average for six experiments where reaction conditions were varied and yielded the following mutant frequencies: 5 mM $MgCl_2$, 10 μM dNTPs: 32%; 5 mM $MgCl_2$, 100 μM dNTPs: 37%; 10 mM $MgCl_2$, 1 mM dNTPs: (18 nM pol-η) 39%, (36 nM pol-η) 37%, (72 nM pol-η) 28 and 32%. In each case, about 1,000 total plaques were scored.
† Error rates for the other DNA polymerases[14,15,27,28] are averages, which vary depending on the mismatch and its location.
‡ Control values are for DNA substrates not subjected to copying *in vitro*.
§ From ref. 16.
‖ The value for exonuclease-deficient Klenow fragment[14].